Nano Select

WILEY-VCH

nano select

RESEARCH ARTICLE OPEN ACCESS

Intratracheal Administration of Nanoplastics With Varying Surface Hydrophobicity Results in Coarsely Vacuolated Alveolar Macrophages, Transient Respiratory Inflammation, and Mild Collagen Deposition

Anna Babin Morgan[1] | Yanira Riffo-Vasquez[2] | Aateka Bodhaniya[3] | Stuart A. Jones[2] | Ben Forbes[2] | Kavitha Sunassee[4] | Rafael T. M. de Rosales[4] | Stephanie Wright[5] | Clive Page[2] | Lea Ann Dailey[6]

[1]Kingston University, Kingston-upon-Thames, London, UK | [2]Institute of Pharmaceutical Science, King's College London, London, UK | [3]School of Life and Medical Sciences, University of Hertfordshire, Hatfield, Herts, UK | [4]School of Biomedical Engineering and Imaging Sciences, King's College London, St Thomas Hospital, London, UK | [5]School of Public Health, Imperial College London, Sir Alexander Fleming Building, South Kensington Campus, London, UK | [6]Department of Pharmaceutical Sciences, University of Vienna, Vienna, Austria

Correspondence: Lea Ann Dailey (leaann.dailey@univie.ac.at)

Received: 29 August 2024 | **Revised:** 22 December 2024 | **Accepted:** 14 January 2025

Funding: This work was supported by funding from, the European Union Horizon 2020 project IMPTOX (#965173), the C. W. Maplethorpe Trust and the Wellcome Trust.

Keywords: hydrophobicity | inflammation | lung | macrophages | nanoplastics

ABSTRACT

Inhalation of biopersistent nanoplastics may have adverse effects on lung health. By varying the acetate content of poly(vinyl acetate-co-alcohol) (PVAc), model nanoplastics with different surface hydrophobicity can be produced to study the effects of nanoplastic hydrophobicity in the lung. PVAc nanoplastics with a high hydrophobicity, administered by oropharyngeal aspiration to C57BL/6j mice (300 μg; ~10 mg/kg), show transient pulmonary inflammation which peaks at 24 h post-administration and resolves by day 7. Hydrophilic PVAc induces no inflammatory effects at the same dose. Pulmonary administration of hydrophilic and hydrophobic PVAc nanoplastics increases the prevalence (~30%–35%) of distinctive coarsely vacuolated alveolar macrophages over 28 days. Hydrophobic PVAc and silica nanoparticles (control) induce minor increases in collagen deposition, but do not stimulate tissue remodeling to the same extent as a bleomycin model of fibrosis. Longitudinal micro-CT imaging is explored as a non-invasive methodology for detection of lung fibrosis. A bespoke image analysis method to quantify high density tissue signal volume correlates moderately well with histopathology-derived collagen deposition data ($R^2 = 0.73$). In summary, inhaled nanoplastics with high surface hydrophobicity induce transient inflammation following a single administration of 300 μg, an increase in coarsely vacuolated macrophages and mild increases in collagen deposition.

1 | Introduction

A public and regulatory interest in the potential of adverse effects following inhalation of respirable micro- and nanoplastics [1–3], has led to an increased number of reports assessing the pulmonary and systemic toxicity of inhaled polymeric nanomaterials. Recently, Yang et al. reported that non-modified polystyrene (PS) nanoparticles (50 nm) administered to the lungs of mice as

This manuscript is dedicated to Domenico Spina, who was a valued and integral member of the team.

an aerosolized aqueous nanoparticle dispersion at doses of 16, 40, and 100 μg/day for 1, 5, and 14 weeks induced dose-dependent pulmonary inflammation and symptoms similar to that seen in chronic obstructive pulmonary disease (COPD) in all treatment groups [4]. Woo et al. [5] similarly reported that intratracheal instillation of 1, 2.5, or 5 mg/kg polypropylene (PP) nanoplastics (0.66 ± 0.27 μm in size; dispersed in saline solution), five times per week for 4 weeks, resulted in lung inflammation putatively mediated by the p38- NF-κB pathway as a result of mitochondrial damage. In a further study of murine responses to the pulmonary administration of nanoplastics, Ji et al. reported that the adverse pulmonary effects of milled nanoplastics—comprised of polyethylene terephthalate (PET), polyvinyl chloride (PVC), and polyethylene (PE) (~100 nm)—were typically more pronounced than commercially available spherical polystyrene particles of the same size. Furthermore, PVC induced slightly more severe lung toxicity profiles compared to the other plastics, and the adverse effects of nanoplastic exposure were comparable to those observed with silicon dioxide (SiO_2) and anatase titanium dioxide (TiO_2) [6]. Although these studies explore the lung toxicity of different plastic types, exposure doses, and durations, they all contribute to a growing evidence base that accumulation of biopersistent plastics in lung may contribute to a chronic pro-inflammatory state in the lung. The unique physicochemical properties of plastics compared to other types of nanomaterials (e.g., silica dust and titanium dioxide), are currently an under-investigated topic. Specifically, the higher surface hydrophobicity of plastics may contribute to a different toxicity profile in the lung [7, 8].

Hydrophobic molecular motifs or surfaces are recognized by the innate immune system as a non-specific danger-associated molecular pattern (DAMP) because, under physiological conditions, hydrophobic regions in endogenous molecules and tissues are typically inaccessible to immune cell recognition receptors [9]. While challenging to demonstrate quantitatively, several studies have shown that nanoparticles with increased surface hydrophobicity elicit an enhanced immune response in both in vitro and in vivo models. For example, Moyano et al. intravenously administered gold nanoparticles (5 mg/kg) coated with headgroups of increasing partition coefficient (log p) values to mice and measured cytokine gene expression patterns in extracted splenocytes. Increasing the headgroup log p value (0.6–5.4) and therefore the surface hydrophobicity of the material correlated with subsequent increased pro-inflammatory cytokine expression (e.g., TNF-α, IFN-γ, IL-2, and IL-6) [10].

Jones et al. [7] and Dailey et al. [8] explored the acute effects of increasing nanoparticle surface hydrophobicity on lung biocompatibility following pulmonary administration (220 cm^2 surface area dose per lung) in Balb/c mice. In these two studies, a range of different nanomaterials (lipid, protein, and polymeric) with increasing surface hydrophobicity were assessed. Following intratracheal administration of a coarse aerosol using a Microsprayer device, two hydrophobic polymer nanomaterials comprised of non-modified PS (50 nm) and poly(vinyl acetate-co-alcohol) (PVAc; 150 nm; dose ~500 μg) induced an acute inflammatory response, characterized by neutrophil infiltration, elevated pro-inflammatory cytokines, and elevated protein levels in the broncho-alveolar lavage (BAL) fluid. It was also observed that exposure to both hydrophobic and more hydrophilic polymeric nanomaterials was associated with increased numbers of alveolar macrophages with unusually large vacuoles in the cytoplasm, while non-polymeric nanomaterials, that is, lipid- or protein-based nanoparticles, did not induce this macrophage response [7, 11, 12].

PVAc is a non-biodegradable plastic used in cosmetics, adhesives, resins, and for laminating metal foils [13]. It also finds extensive applications in the shipbuilding industry and is a component of microplastics found in marine sediments [14]. It has been identified in storm drain retention ponds, albeit in a much lower prevalence than other common plastics [15]. In our previous works [7, 8, 16], PVAc was used as a model polymer to assess the effect of surface hydrophobicity on respiratory toxicity, because it may be modified by controlled saponification to hydrolyze the PVAc ester side groups, resulting in copolymers with different hydrophobicity based on their acetate:alcohol mol ratio (Figure 1A) [17, 18]. Intriguingly, Jones et al. reported that PVAc nanoparticles with a high acetate:alcohol mol ratio of ~80:20 (PVAc80%) were highly pro-inflammatory and associated with lower numbers of coarsely vacuolated alveolar macrophages (~20%), while the more hydrophilic PVAc nanoparticles with an acetate:alcohol mol ratio of ~60:40 (PVAc60%) were non-inflammatory under the same conditions. In contrast, the more hydrophilic PVAc nanomaterials induced a vacuolated phenotype in approximately 50% of the BAL macrophages [7]. Further in vitro investigations of PVAc60% in the J774 macrophage-like cell line demonstrated that the nanoparticle-induced macrophage vacuolation was not associated with phospholipid accumulation and therefore could not be classified as phospholipidosis. Interestingly, the PVAc60%-induced vacuolated cells showed a slightly lower metabolic activity, but were otherwise capable of normal phagocytosis, showed unimpaired response to lipopolysaccharide challenge and had no apoptosis markers, that is, elevated caspase 3/7 [19].

The unexpected observations following single-administration lung exposure to the two grades of PVAc nanomaterials stimulated the following questions: How long do these abnormal, highly vacuolated macrophages reside in the lung? Does the PVAc-induced inflammation persist or resolve over time? Are both grades of PVAc nanoparticles associated with lung pathologies, such as fibrosis, which require a longer time frame for development and resolution? To address these questions, a 28-day study in C56BL/6j mice following a single-dose administration of hydrophilic and hydrophobic PVAc nanoparticles was performed and the following parameters of respiratory toxicity were assessed: the presence of coarsely vacuolated macrophages, pro-inflammatory responses, and elevated collagen deposition (Figure 1B). Silica quartz dust (Min-U-Sil 5) was included as a comparator nanostructured material known to cause elevated collagen deposition and pulmonary fibrosis (i.e., silicosis) over time [21]. Additionally, bleomycin treatment was also used as a positive control for fibrosis development [22, 23].

Parallel to assessment of conventional toxicity parameters in BAL and tissue, a non-invasive micro-computed tomography (micro-CT) imaging technique was used to assess a subset of treated animals throughout the study period (Figure 1B). Although magnetic resonance imaging (MRI) is used more routinely in clinical settings for detecting soft tissue changes [22–25], micro-

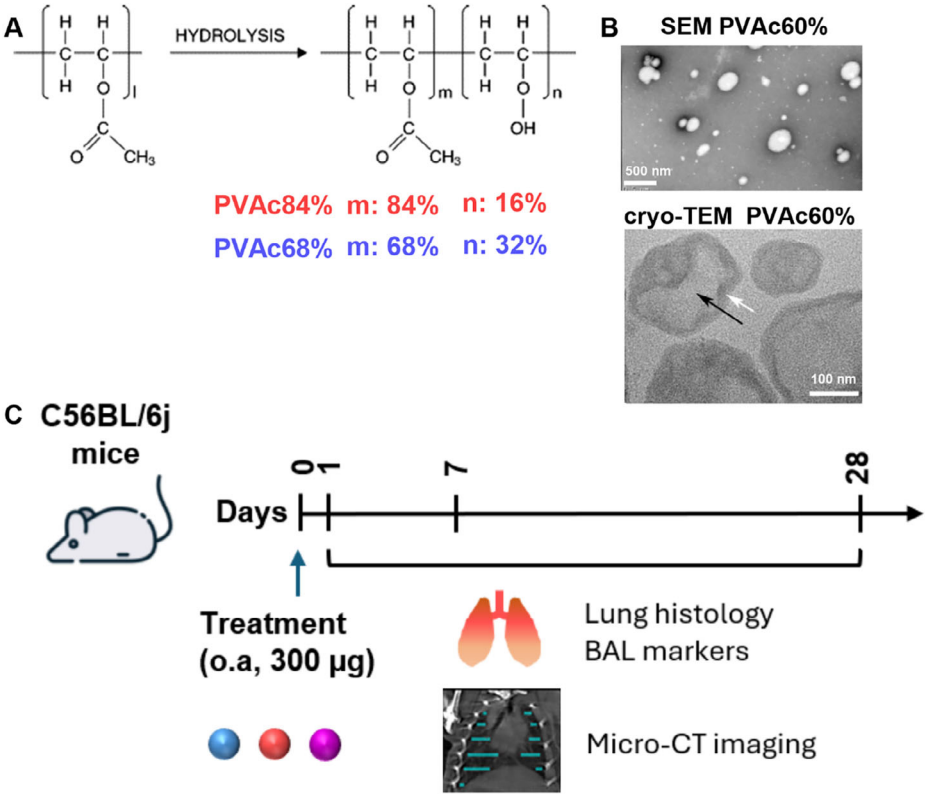

FIGURE 1 | (A) Poly(vinyl acetate-co-alcohol) (PVAc) with different acetate:alcohol ratios can be produced via controlled hydrolysis of poly(vinyl acetate). The ratios use in the current study are PVAc84% (84% acetate:16% alcohol) and PVAc68% (68% acetate:32% alcohol). (B) Scanning electron microscopy (SEM; [17]) and cryo-transmission electron microscopy (cryo-TEM; [20]) images of representative PVAc60% nanomaterials from previous studies (reprinted with permission). The black arrows in the cryo-TEM image indicate the PVAc core and the white arrows indicate the polyvinyl alcohol coating adsorbed to the surface for colloidal stability. (C) Schematic of the current study to assess lung toxicity following a single oropharyngeal aspiration (o.a.) administration of nanomaterials (300 µg) to the lungs of C56BL/6j mice following by analysis of lung histology, markers of inflammation and tissue damage in the lavage fluid, as well as noninvasive micro-CT imaging.

CT was chosen as the imaging modality in this study, due to its more widespread availability in research lab settings. The micro-CT analysis used here is based on imaging the thoracic region of the mouse before and after treatment, then quantifying the total tissue volume (mm^3) associated with a high-density signal recorded in Hounsfield units (HU). In a soft tissue system, the Hounsfield unit scale typically ranges from 0 HU (signal density of water) to −1000 HU (signal density of air). In the healthy lung, the parenchyma typically shows signal values ranging between −1000 and −50 HU, while high-density structural features, such as larger airways, have signal values ±300 HU [26–28]. It was hypothesized that pathologies that increase tissue density, such as inflammation, edema, or collagen deposition, would be detectable via an increase in tissue volume with a high-density signal (i.e., ±300 HU), providing a longitudinal and noninvasive measure of nanoparticle-induced changes to the lung.

2 | Results

2.1 | Polymer and Nanoparticle Characterization

Nuclear magnetic resonance (NMR) analysis of the PVAc solid polymers used in the current study showed mean hydroxylation values of 31.9 ± 1.4% mol:mol for the more hydrophilic PVAc polymer (molecular weight: 13 kDa; $n = 7$), and 16.2 ± 1.7% mol:mol for the more hydrophobic PVAc polymer (molecular weight: 48 kDa; $n = 5$). This difference was considered highly significant ($p < 0.001$); therefore, polymers were understood to differ significantly in their degrees of hydroxylation as a measure hydrophobicity [7]. The respective polymers are abbreviated with their molar content of hydrophobic acetate residues: PVAc84% (84% acetate:16% alcohol groups) and PVAc68% (68% acetate:32% alcohol groups) (Figure 1A). Nanoparticles were prepared from the PVAc polymers by injection of a methanolic polymer solution into an aqueous solution containing 0.33% w/v polyvinyl alcohol (PVA) under continuous stirring and subsequent evaporation of the methanol. PVA is a low molecular weight (10 kDa) water-soluble polymer required for colloidal stability in aqueous media. Dynamic light scattering measurements showed that PVAc68% and PVAc84% nanoplastics did not differ significantly in size and all dispersions were stable in their respective dosing vehicles (Table 1). Zeta potentials for both PVAc dispersions were neutral, while silica demonstrated a markedly negative value.

2.2 | Rationale for the Choice of Administered Dose

The choice of dose was based on earlier seminal studies with non-modified PS beads of various sizes (i.e., 64, 202, and 535 nm), which showed that nanoparticle surface area dose correlated

TABLE 1 | Mean hydrodynamic diameters of nanomaterials in deionized water or vehicle (* sterile 5% dextrose solution; ** sterile PBS) and zeta potential measured in 6.3 mM NaCl (mean ± standard deviation, $n = 6$).

	Hydrodynamic diameter in deionized water (nm)	Hydrodynamic diameter in dosing vehicle (nm)	ζ-potential (mV)
PVAc68%	167 ± 11	177 ± 13*	−4.80 ± 0.38
PVAc84%	166 ± 26	175 ± 23*	−6.96 ± 0.24
Silica	625 ± 154	727 ± 162**	−50.9 ± 2.34

better with pulmonary inflammation metrics compared to mass-based doses values [29–30]. In Jones et al. we also observed this phenomenon, when similar levels of lung inflammation were detected following the administration of 220 cm^2 hydrophobic PVAc nanomaterials (150 nm; 500 μg/lung) and non-modified PS (50 nm; 200 μg/lung). At lower surface area doses (22 cm^2; 50 and 20 μg/lung, respectively) only negligible inflammatory effects were observed for both hydrophobic nanoplastics [7]. Intriguingly, no inflammatory effects were observed after administration of hydrophilic PVAc nanoparticles at both 22 and 220 cm^2, indicating that surface hydrophobicity of nanoplastics is an important driver of lung inflammation [7]. In the current study, we chose to administer the PVAc nanoplastics at an intermediate dose of 300 μg/lung (~100 cm^2, ~10 mg/kg) because it was of interest to explore the effects of PVAc nanoplastics at a lower dose, while still maintaining the pro-inflammatory profile of hydrophobic PVAc nanomaterials to assess whether this response is detectable with the noninvasive micro-CT imaging method. Furthermore, silica particles administered in this dose range have previously been reported to induce low-level inflammation and increased collagen deposition over longer study periods [21]. It should therefore be emphasized that the doses chosen are not meant to reflect realistic environmental or occupational exposure levels to respirable micro- and nanoplastics.

2.3 | Assessment of Lung Inflammation, Tissue Damage, and Vacuolated Macrophages

In the current study, both the PVAc nanoplastics produced the same responses as in previous studies [7, 8], whereby the more hydrophobic PVAc84% nanoplastics induced an acute inflammatory response in the mouse lung with increased numbers of polymorphonuclear cells (PMNs) and elevated levels of pro-inflammatory cytokines (e.g., TNF-α and IL-6) detected in the BAL fluid at day 1 (Figure 2). This type of response profile is characteristic of a general pro-inflammatory response of the lung toward a variety of engineered nanomaterials and many studies have found evidence that nanoparticles induce lung inflammation by activating various cell signaling pathways such as TRPM2, IL-1α, NFκB, PKC-α, and EGFR [31]. In contrast, the more hydrophilic PVAc68% nanoparticle suspension showed a minimal response, that is, only minor elevations in PMNs 1-day post-dosing. All measures of acute inflammation observed in BAL after PVAc84% nanoplastic exposure resolved by day 7.

A separate group of mice were treated with a regime of low-dose chronic bleomycin, a glycopeptidic antibiotic and antineoplastic compound known to induce lung injury and fibrosis [22, 23]. Bleomycin-induced weight loss was commensurate with known treatment effects but this did not exceed 20% body weight. No animals were euthanized for bleomycin-induced weight loss, and no weight loss was observed in any other groups. The BAL analysis for the bleomycin treatment group showed inflammation and evidence of tissue damage in terms of increased levels of BAL protein (Figure 2), which were consistent with previous reports on the effects of bleomycin in mice [31, 33]. In comparison, the administration of 300 μg finely ground silica to the lungs resulted in mild inflammation as characterized by elevated BAL neutrophils (Figure 2). This response to silica treatment was lower than expected and may have represented strain-related differences in comparison to those reported in other murine models of silica-induced lung injury [21].

Tissue histopathology was assessed at days 1, 7, and 28 (Figure 3), with the results largely reflecting the indicators of inflammation and tissue damage measured in the BAL fluid. No evidence of macrophage accumulation, vacuolation, neutrophil infiltration, or tissue damage was observed in the saline vehicle or PVAc68% treatment groups. PVAc84% treatment resulted in a dense accumulation of macrophages and PMNs in the tissue regions surrounding the central airways (although less so in the periphery of the airways) at day 1, which fully resolved by day 7. Silica treatment resulted in very minor tissue changes, predominately the observation of accumulations of enlarged alveolar macrophages with evidence of mild neutrophilia in the central airways increasing from days 1 to 28. Finally, bleomycin treatment resulted in substantial changes to the tissue from day 1 with increasing severity on days 7 and 28. The density of tissue staining resulting from inflammatory cell accumulation and tissue remodeling was evident at all timepoints post-bleomycin administration.

In addition, it was previously observed that both PVAc nanoparticle treatments were associated with high levels of coarsely vacuolated mononuclear cells (MNCs), most of which are assumed to be alveolar macrophages [7, 19]. This phenomenon was also observed in the current study following PVAc nanoparticle treatment (Figure 4). The percentage of coarsely vacuolated MNCs was determined by counting the prevalence of abnormally vacuolated cells (with morphology similar to the cells shown in the micrographs in Figure 4B) within a population of 100 cells. Elevated numbers of coarsely vacuolated cells were observed throughout the entire 28-day study period, although the prevalence peaked at day 7. Similar to observations reported by Jones et al. [7], the more hydrophilic PVAc68% nanoplastics tended to show a higher prevalence of abnormal MNCs compared to the more hydrophobic PVAc84% nanoplastics, although the difference between the two systems is not significant in this study.

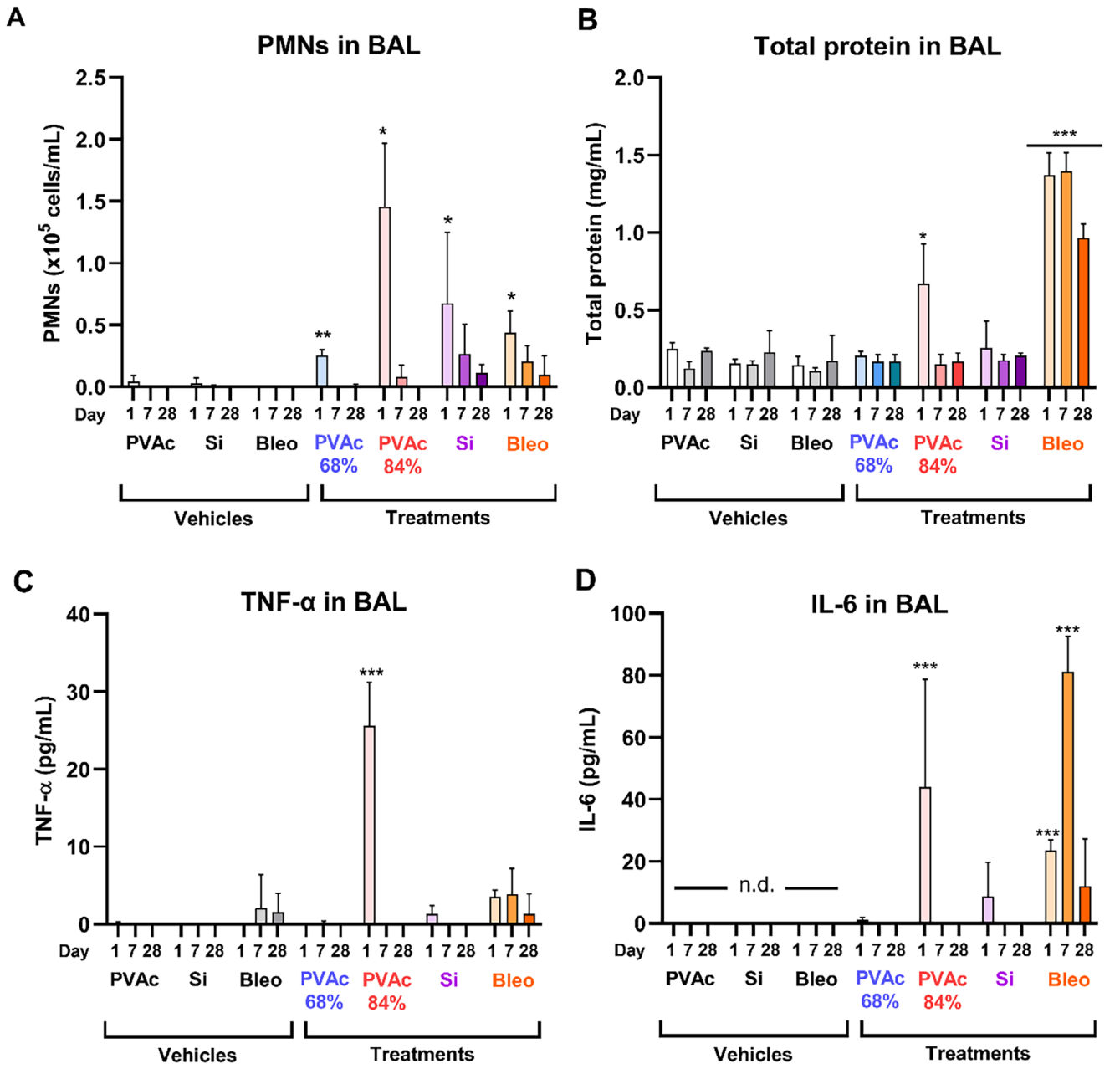

FIGURE 2 | Analysis of lung inflammation and tissue damage in BAL. (A) Number of infiltrating polymorphonuclear cells (PMNs), (B) total BAL protein content (mg/mL), (C) BAL TNF-α concentration (pg/mL), and (f) BAL IL-6 concentration (pg/mL). Values represent the mean ± standard deviation from $n = 3$–4 animals per group per time point. Three vehicle controls (represented in gray tones) were used: PVA (0.4 mg/mL) in 5% dextrose (PVAc vehicle), PBS (silica nanoparticle vehicle), and isotonic saline (bleomycin vehicle). (*$p < 0.05$, **$p < 0.01$, ***$p < 0.001$; sample vs. matched vehicle at each respective time point). n.d. = not detected.

2.4 | Assessment of Lung Edema and Collagen Deposition

Wet and dry lung weights were recorded for standard gravimetric analysis to evaluate whether treatments induced edema. Edema was characterized as an increase in the ratio of wet/dry lung weight and a minor but significant increase was only observed in the bleomycin-treated group on day 1 ($p < 0.05$), compared to naïve animals (Figure S1A). A comparison of lung dry weights (Figure S1B) revealed that a significant increase in mass was also observed for the bleomycin-treated group, indicating collagen deposition with remodeling but was not observed for other treatment groups. This was further investigated through collagen-specific staining using picrosirius red (Figure 5), revealing that bleomycin-treated animals showed extensive collagen deposition and tissue damage from day 1 onwards, while this was not as evident for the nanoparticle treatment groups.

A semi-quantitative image analysis was performed with picrosirius red stained samples (20× magnification), whereby total collagen deposition was expressed as the picrosirius factor (PF%; Figure 5). The PF% was derived by capturing a total of 39 non-overlapping images (0.6 mm^2 each) from cryo-slices taken from different lung lobes of each animal. The extent of collagen

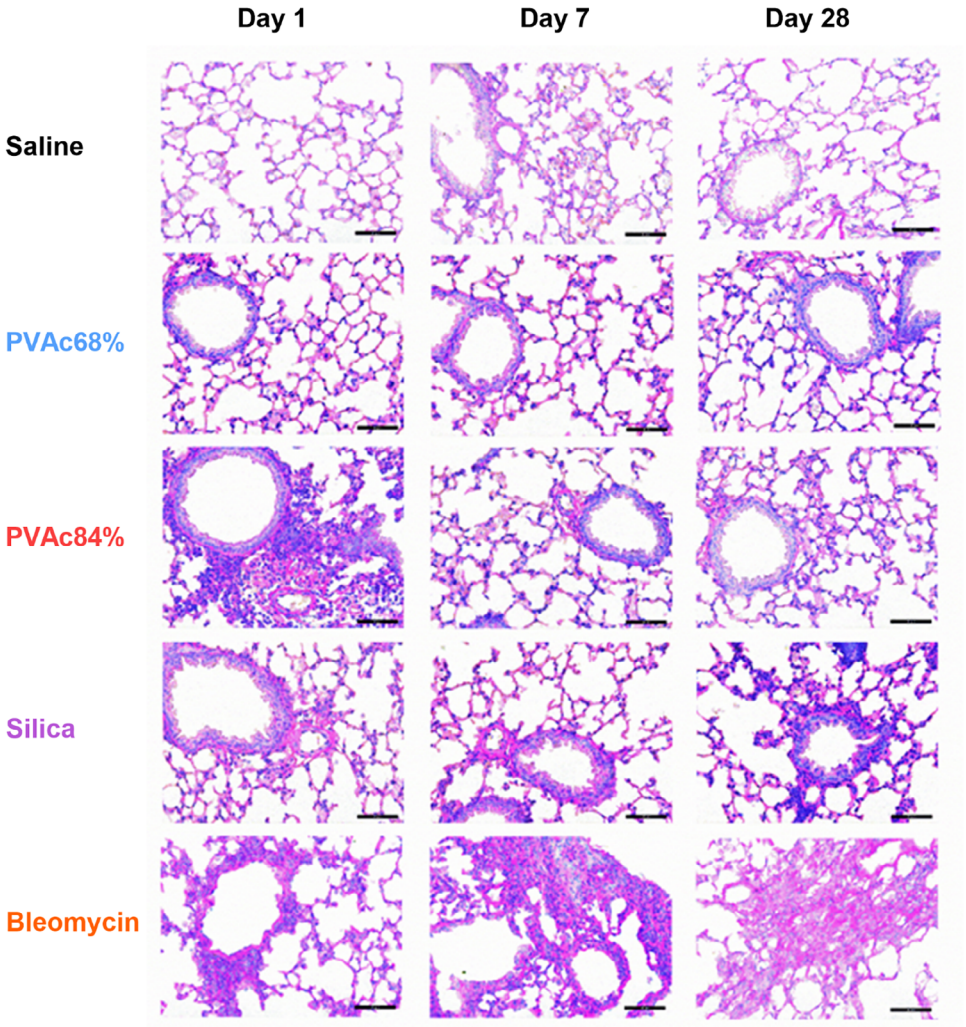

FIGURE 3 | Tissue histopathology at days 1, 7, and 28 post-administration of saline vehicle, PVAc68% nanoparticles, PVAc84% nanoparticles, silica, or bleomycin. Representative images of hematoxylin and eosin (H&E) stained tissue slices were taken at 40× magnification. Black scale bars denote a length of 50 μm.

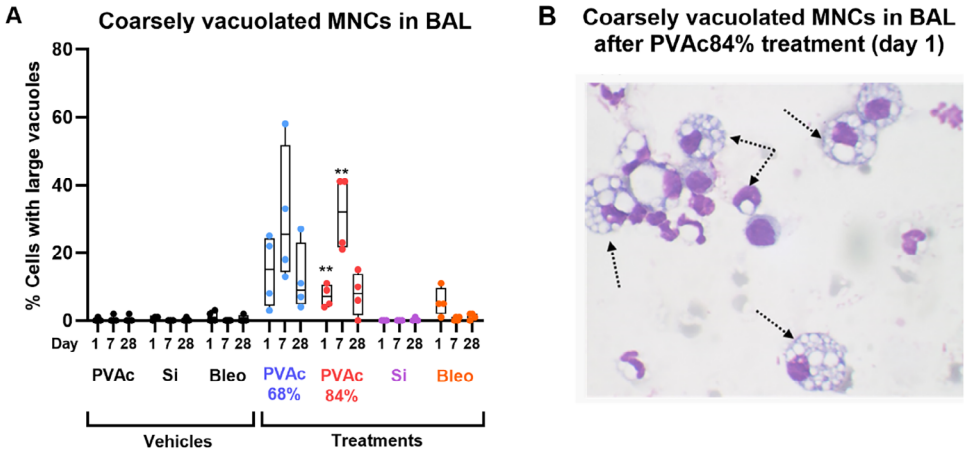

FIGURE 4 | Percentage of coarsely vacuolated mononuclear cells (MNCs) at days 1, 7, and 28 post-administration of vehicles, PVAc68% nanoparticles, PVAc84% nanoparticles, silica, or bleomycin. A box and whiskers plot shows the central quartiles, median, minimum, and maximum values from $n = 3$–4 animals per group per time point. (B) Microscope images of the BAL cellular fraction stained with Reastain Quick-Diff Kit (Reagena Ltd, Finland) and taken at a 100× magnification. The sample shown was taken from a mouse treated with PVAc84% nanoplastics at day 1 post-administration.

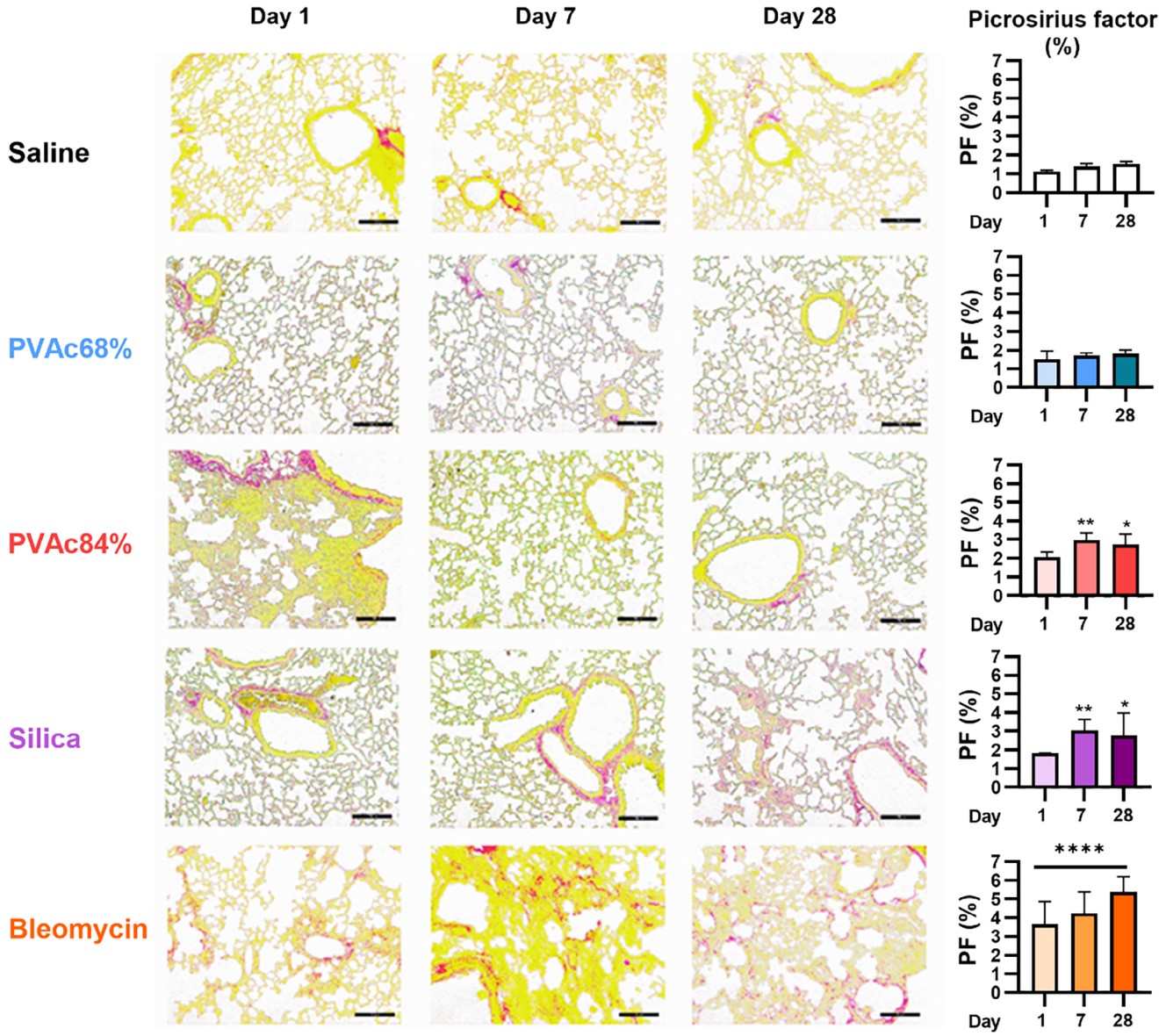

FIGURE 5 | Lung tissue stained with picrosirius red at days 1, 7, and 28 post-administration of saline vehicle, PVAc68% nanoparticles, PVAc84% nanoparticles, silica, or bleomycin. Representative images of picrosirius red-stained tissue slices were taken at 20× magnification. Black scale bars denote a length of 100 μm. The panel of graphs to the right of the micrographs depict the picrosirius staining factor (PF%) calculated by ImageJ from $n = 4$ animals (mean ± standard deviation). *$p < 0.05$, **$p < 0.001$, ****$p < 0.0001$; compared to time-matched saline control groups.

staining (i.e., red signal) in each 0.6 mm^2 image was quantified using the ImageJ threshold tool (ImageJ software). From the 39 images, the region with the lowest red intensity value, typically associated with non-collagenous tissue, was designated as a background and subtracted from all other areas to normalize the staining intensity values. Normalized intensities for all 39 sections were summated, divided by the total image area, and multiplied by 100 to yield a PF% value for each animal. Interestingly, PVAc84% and silica nanoparticle-treated animals also showed minor, but significant increases in PF% at days 7 and 28. Lung slices of PVAc68% treated animals resembled those of the saline control group. Significantly elevated PF% values were observed for bleomycin treatment groups at all time points, reflecting visible patterns observed in the tissue histopathology.

2.5 | Micro-CT Assessment of Longitudinal Respiratory Toxicity

Longitudinal micro-CT assessment of freely breathing mice was performed on days 0, 1, 7, and 28 to track changes in lung health following the different treatments. Since image quantification from the whole lung significantly increased analysis time and masked regio-specific high-density signals potentially indicative of pathologies, an alternative approach using the evaluation of six evenly spaced transverse image slices was investigated as a surrogate for the whole lung (Figure 6A). The average tissue density for whole lung data sets (−451 ±55 HU/voxel) was very similar to the average signal from the six transverse image slices (−480 ±65 HU/voxel) and both values were in the expected range for parenchymal tissue values (Figure 6B) [34], indicating

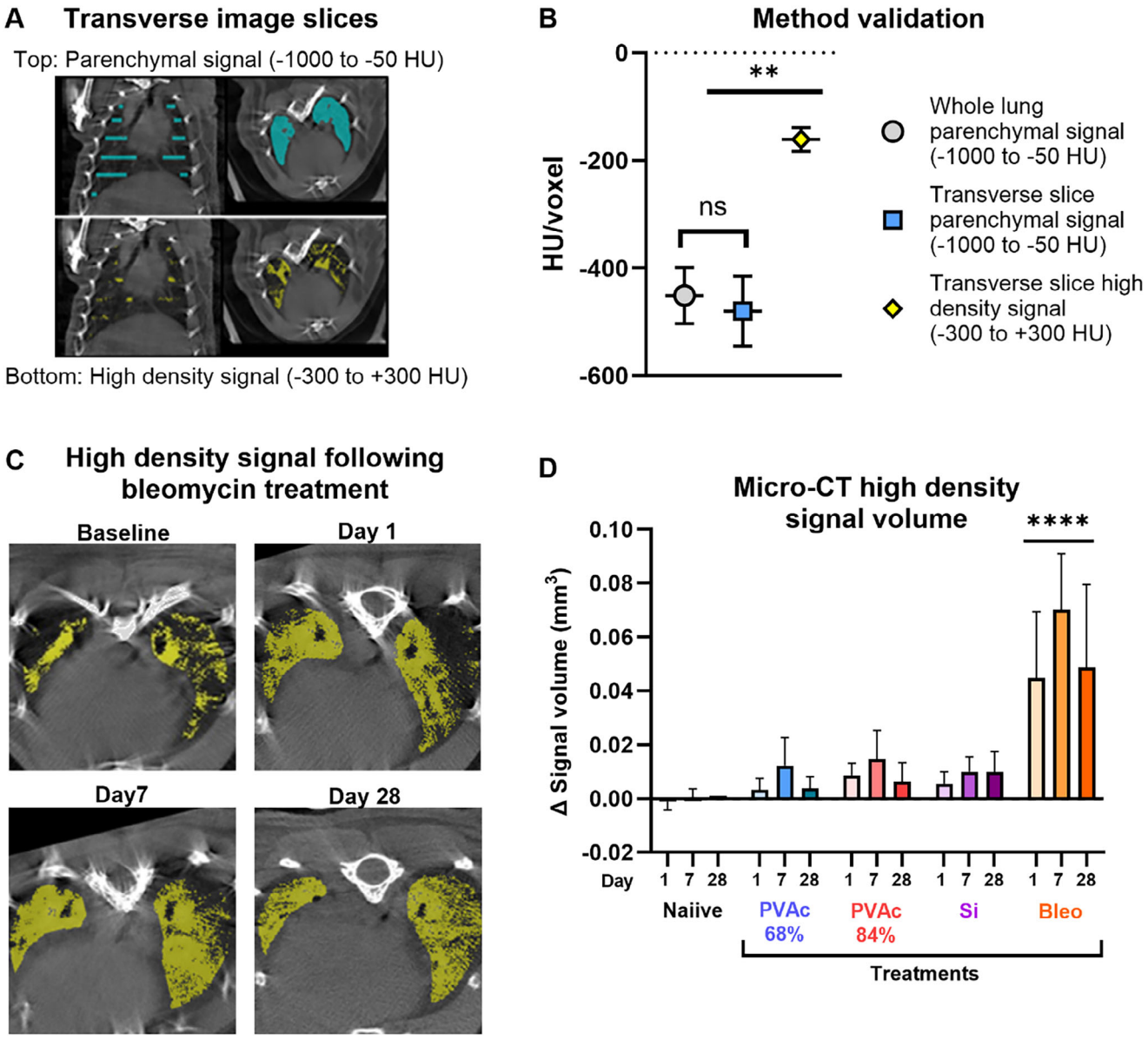

FIGURE 6 | (A) Parenchymal versus high-density signals in naïve mice: Micro-CT acquired images of six transverse sections of a naïve mouse lung. The top panel shows the average parenchymal signal density (HU/voxel) when measurements were restricted to 1000 to −50 HU. The bottom panel shows average high density signal values (HU/voxel) measured between −300 to +300 HU. High attenuation artifacts (e.g., bone) were excluded from all analyses. (B) Comparison of average parenchymal signal density values calculated from whole lung measurements (gray) versus values calculated from six transverse slices (blue). These are compared with average high density signals calculated from six transverse slices. Values represent the mean ± standard deviation from $n = 4$ naïve mouse lungs. $^{**}p < 0.001$. (C) Images of the high density signal development in a single mouse following bleomycin treatment. (D) Average high density signal volumes calculated from six transverse slices ($n = 4$ animals). $^{****}p < 0.0001$ compared to matched time points in the naïve group.

that the alternative analysis protocol was representative of the whole lung. The further analysis detected a significant difference in the average tissue density recorded using the parenchymal measurement range (−1000 to −50 HU) compared to high-density measurement range of −300 to +300 HU (−161 ± 22 HU/voxel, $p < 0.01$) (Figure 6B), which confirmed that despite the overlap in measurement range, the analysis approach was able to quantify parenchymal values as distinct from surrounding high density values understood to represent the relatively denser vasculature and supporting architecture in the lungs of naïve mice. The ability to distinguish non-parenchymal values as separate from parenchymal values made high density regions a suitable marker for the longitudinal tracking of changes associated with increased tissue density such as inflammation, collagen deposition, fibrosis, and/or angiogenesis [22, 23].

Longitudinal quantification of high density regions was performed and the baseline value subtracted from each time point to provide a mouse-specific change in high density signal volume over time (Δ mm^3; Figure 6D). The Δ mm^3 in naïve mice was not significantly altered over time (negative control), while a large and significant increase Δ mm^3 was observed at all time points

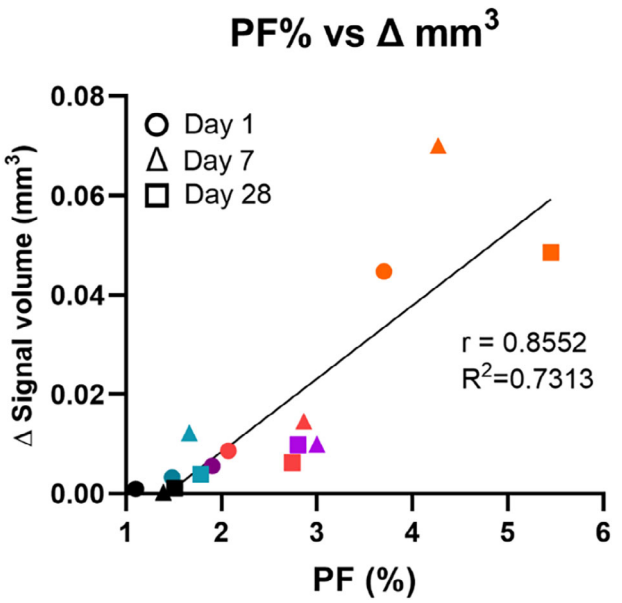

FIGURE 7 | Mean PF% values from collagen deposition studies were plotted against micro-CT-derived Δ mm^3 values from animals in negative control groups (black symbols), or treated with PVAc68% nanoplastics (blue), PVAc84% nanoplastics (red), silica nanoparticles (purple) and bleomycin (orange) at day 1 (circles), day 7 (triangles) and day 28 (squares). Values for the Pearson correlation (r) and coefficient of determination (R^2) are shown.

following bleomycin treatment (positive control; Figure 6C). This difference indicates that the longitudinal quantification of high-density signal volumes is able to correctly distinguish between healthy lungs and those with extensive tissue damage.

This quantification protocol was next applied to the post-acquisition image processing of the nanoparticle treatment groups: PVAc68%, PVAc84%, and silica (Figure 6D). Treatment with nanomaterials resulted in minor increases in Δ mm^3, but these were not significant compared with the naïve control group. It was of interest to examine whether the high density signal volume measured by micro-CT corresponded to levels of collagen staining, which would provide an indication that the micro-CT signal is driven by collagen deposition in response to treatment. A correlation plot of the picrosirius factor (PF%) versus the high-density signal volume (Δ mm^3; Figure 7) showed a moderately good Pearson correlation value ($r = 0.8552$) and coefficient of determination ($R^2 = 0.7313$). The Δ mm^3 was not highly correlated to any other singular parameter measured (data not shown).

3 | Discussion

The current study was designed to investigate adverse respiratory responses to PVAc nanoplastic exposure by quantifying the extent of inflammatory and/or fibrotic changes observed over 28 days following a single pulmonary administration. Furthermore, this study sought to quantify the persistence of coarsely vacuolated macrophages over time and investigate differences resulting from the mouse strain in comparison to previous studies (i.e., C56BL/6j in the current study vs. Balb/c in [7]), as well as explore noninvasive longitudinal micro-CT imaging as a method for assessing lung tissue damage following nanoparticle exposure.

The comparisons to prior research using PVAc nanomaterials revealed that the overall cellularity in the BAL of C57BL/6j mice was lower than that of BALB/c mice studied previously [7], although data trends remained the same, with the more hydrophobic nanoplastics inducing a transient pro-inflammatory response, while the more hydrophilic PVAc nanomaterials did not. Taken together, the results of this study are in line with a growing body of literature linking nanomaterial hydrophobicity to toxicity in vitro and in vivo, across a range of organic and inorganic nanomaterials [7, 8, 10, 35–37].

Intriguingly, the prevalence of coarsely vacuolated MNCs in the BAL fluid does not appear to be directly linked with nanoparticle hydrophobicity or inflammation, as vacuolated cells were observed after exposure to both PVAc particle types and remained prevalent in the lungs over 28 days. Furthermore, this highly vacuolated macrophage response appears to be associated primarily with nanoplastic exposure, since finely ground silica nanoparticles did not induce a similar response in this study. Jones et al. also found coarsely vacuolated macrophage populations in the BAL of animals exposed to nanoplastics (PVAc and PS) but not in animals exposed to protein or lipid-based nanomaterials [7]. Interestingly, the coarsely vacuolated macrophages were only observed in the cellular fraction of the BAL fluid and could not be found in the parenchymal tissue slices, which are typically used for routine toxicology assessment. The underlying mechanism and the long-term implications of this vacuolated phenotype are currently not well understood, although Hoffman et al. have identified that PVAc-treated cells do not stain positive for elevated phospholipid content [19], indicating that phospholipidosis [38] is likely not occurring in this cell population. Elevated neutral lipid levels were observed [19]. Rather, it may reflect either the early stages of apoptosis or dysfunctional autophagy, as has been postulated for a wider variety of nanoparticles [39–42].

In addition to inflammation, the current study sought to explore any fibrotic-associated effects of single-dose nanoparticle treatment, as quantified by picrosirius red staining for collagen deposition and micro-CT imaging. The longitudinal investigation revealed that lungs exposed to saline and the more hydrophilic PVAc68% nanoplastics showed low levels of collagen deposition (PF% ~1%), while collagen deposition was elevated to a minor but significant extent in lungs exposed to the more hydrophobic PVAc84% and silica nanomaterials (PF% = 2%–3%). When compared to chronic bleomycin for the induction of fibrosis (PF% > 4%), a single administration of nanomaterials appeared to result in relatively mild tissue changes with no notable tissue remodeling. As both the total dose and length of exposure are known to influence bleomycin-induced lung injury [22, 23], these findings may highlight that chronic exposure to hydrophobic polymeric nanomaterials could result in a fibrotic respiratory toxicity over the longer term. The inclusion of collagen deposition as an endpoint in chronic exposure studies with environmentally relevant concentrations of nanoplastics could therefore be useful.

Changes in the lungs were also tracked using micro-CT as an adjunct (noninvasive) methodology compared to conventional (invasive) nanotoxicology assessments. The micro-CT image

analysis method developed was based on the quantification of the high-density values from six representative transversal lung regions of interest. A moderately good correlation was revealed between high-density signal volumes and the PF%, indicating that the micro-CT image analysis has the potential as an indicator of collagen deposition and fibrosis development in the lungs, although the technique could benefit from further investigation and refinement. It was, for example, noted that micro-CT imaging was not able to detect increased tissue density resulting from the lung inflammation present at day 1 following PVAc84% nanoparticle exposure, as was clearly seen in the H&E histopathology. It may be that cellular infiltration was not detectable within the focused range of ±300 HU but may be quantifiable within a different range relative to the specific micro-CT attenuation achieved. Tissue histopathology also indicated that PMN infiltration was localized in the upper and central regions of the lung, reflecting the likely distribution pattern of nanomaterials following oropharyngeal aspiration of a bolus liquid [43]. Therefore, the analysis of high-density volumes in the six evenly spaced transversal sections may have underrepresented the density changes occurring only in the upper regions of the lung. It is anticipated that advanced image processing methods, such as texture analysis, combined with machine learning, may be able to provide more detailed and sensitive information regarding respiratory tract changes measured using micro-CT [44–47].

In addition, it was noted that longitudinal studies using invasive methods such as ventilation, gating, or using postmortem image analysis, to derive images with greater anatomical clarity and fewer motion artifacts, may also have the potential to capture pulmonary injuries with greater resolution. Such has been seen, for example, in a recent mouse model of pulmonary disease, employing an automated pulmonary air and tissue segmentation protocol with in vivo respiration controlled and breath-gated scanning in combination with post-mortem imaging and ex vivo high-resolution scanning to improve the efficiency and limit user-associated bias in the quantification of pulmonary injury [48]. With adaptability to longitudinal models, such methods could be incorporated in future investigation of pulmonary nanotoxicity but will require greater numbers of animals to be used. A compromise may be to develop a similar protocol in freely breathing animals, forgoing the ventilated and gated aspects but incorporating selected post-mortem imaging and ex vivo high-resolution scanning. Such approaches will be the focus of ongoing investigations to improve the use of longitudinal non-invasive imaging methodology in the field of respiratory nanotoxicology.

4 | Conclusions

This study confirmed that increases in the surface hydrophobicity of PVAc nanoplastics are associated with increased acute inflammatory effects in the mouse lung, which resolves within 7 days after a single administration. Exposure to PVAc nanoplastics led to an increased prevalence of distinctive coarsely vacuolated MNCs in the BAL fluid, which were present over the entire 28-day observation period, although the long-term implications of this observation remain undetermined. The single exposure to hydrophobic PVAc84% nanoparticles also induced a minor, but significant increase in collagen deposition in the lungs, although no evidence of tissue remodeling was observed. Since the effects of cumulative respiratory exposure have yet to be studied and these may reveal more substantial pathology. Finally, longitudinal micro-CT imaging was assessed as a non-invasive adjunct methodology for use in respiratory nanotoxicology studies. Using the image analysis protocol developed for this study, the micro-CT assessment correlated well with the conventional assessment of collagen staining used as a biomarker for fibrosis, but CT was not able to distinguish high levels of cellular infiltration which occurred as part of the inflammatory response. However, future method development in the area of image analysis shows promise for improving the diagnostic specificity of image processing, presenting an attractive platform for the rapid and non-invasive longitudinal assessment of lung health following exposure to nanoplastics.

5 | Experimental Section

5.1 | Materials

Two molecular weight grades of PVAc, high (48 kDa) and low (12.8 kDa), were purchased from Sigma-Aldrich (Dorset, UK). Poly vinyl alcohol (PVA; 8–12 kDa) was purchased from Sigma-Aldrich (Dorset, UK). Fine ground crystalline silica (Min-U-Sil 5 quartz dust) was a gift from the US Silica Company (Houston, TX, USA). Bleomycin A5 hydrochloride was purchased from LKT Laboratories (Cambridge Bioscience Ltd, Cambridge, UK). All other materials were of analytical grade.

5.2 | PVAc Synthesis and Nanoparticle Fabrication

The PVAc polymers were modified by direct saponification as previously detailed by Chana et al. [17]. From the high molecular weight precursor, a modified PVAc polymer with 16 mol% hydroxyl groups and 84 mol% residual acetate groups (PVAc84%) was produced. Modification of the low molecular weight precursor yielded a PVAc polymer with 32 mol% hydroxyl groups and 68 mol% residual acetate groups (PVAc68%). Polymer purity and degree of hydrolysis were verified by NMR analysis [17, 18]. To prepare PVAc nanoparticles, a solution of 5% w/v PVAc68% or 1% w/v PVAc84% polymer in 2:1 methanol:water was injected into 0.33% w/v aqueous PVA under continuous stirring. Following solvent evaporation, suspensions were filtered (0.4 μm syringe filter) and dialyzed against water (>48 h) to remove excess PVA. Purified nanosuspensions were subsequently concentrated using ultrafiltration centrifuge tubes (100 kDa MWCO; Millipore, Watford, UK).

5.3 | Nanoparticle Characterization

PVAc and silica suspensions were investigated to determine hydrodynamic particle size and zeta potential (Zetasizer Nano ZS: Malvern, Worcestershire, UK). Particle size was determined using dynamic light scattering using a scattering angle of 173° with refractive indices and viscosity values optimized per run. Samples were diluted at >0.01 mg/mL in deionized water or dosing vehicle(s) to investigate colloidal stability. PVAc nanoplastics were size-stable when stored in purified water at 4°C. Zeta

potential measurements were performed at 25°C in 6.3 mM saline solution. Data is reported as the mean ± standard deviation of n = 3 nanoparticle batches.

5.4 | In Vivo Pulmonary Administration

All procedures were conducted in accordance with the UK Animals (Scientific Procedures) Act 1986 (Project License Number 70/8279). Male C56BL/6j mice (Harlan, UK) weighing 21–25 g, were allowed no less than 1-week acclimatization before use. Animals were kept under a 12:12 light:dark cycle, in a climate controlled environment with access to food and water ad libitum. Body weight was recorded throughout the study, as a measure of general health.

PVAc nanoparticle suspensions were prepared under aseptic conditions in sterile 5% dextrose solution. Autoclaved silica (quartz dust) was added to sterile phosphate buffered saline (PBS), and suspensions were probe sonicated for 30 min (Jenson Vibra Cell, 50 W/60 Hz). All suspensions were shaken gently immediately prior to use. Bleomycin solution was prepared in sterile filtered saline as 10 mg/mL stock, and aliquots were diluted for dosing. Bleomycin was stored at 4°C for the duration of use.

An adapted oropharyngeal aspiration dosing technique was used for lung administration [44], and doses were chosen to produce a low to mid-range response based on existing literature [7, 21]. Anesthetized mice (isoflurane: 4% in O_2) were briefly suspended by their upper incisors. Fingertip pressure was used to secure the tongue away from the oral cavity to suppress swallowing. The nostrils were gently held closed by fingertip pressure to induce mouth-breathing. Using a micropipette, 40 μL of PVAc or silica suspension (300 μg/mouse), or vehicle, were applied near the posterior pharynx. Aspiration was confirmed by the rapid disappearance of liquid from the opening of the larynx accompanied by simultaneous inspiration of breath. The vehicle control for PVAc nanoparticle suspension consisted of a 5% dextrose solution containing residual PVA stabilizer (<0.4 mg/mL) [7]. As a positive control for lung injury and fibrosis, chronic bleomycin was administered via oropharyngeal aspiration, whereby mice received six applications of bleomycin (0.05 mg/kg body weight) or saline vehicle. The time course for chronic dosing consisted of bleomycin uid for 3 days, followed by a 2-day rest period where no bleomycin was applied. Then a final 3-day course of bleomycin was administered. This provided a total cumulative dose of 7.5 μg/mouse, with the two-day dosing hiatus considered beneficial in reducing the stress of repeated manipulations [22, 23].

5.5 | Assessments of Pulmonary Inflammation and Fibrosis

5.5.1 | Inflammatory Cells, Cytokines, and Protein

Animals were sacrificed 1, 7, and 28 days post-treatment. The common veterinary anesthetic ethyl carbamate (urethane: Sigma-Aldrich, St. Louis, MO, USA) was used in accordance with IARC guidelines [49, 50]. Prior to BAL fluid collection, mice were sacrificed with an intraperitoneal overdose of the anesthetic (urethane 50% w/v in water, >0.3 mL/mouse). The trachea was exposed by a midline incision and cannulated with a 24-gauge plastic tube attached to a 1.0-mL syringe. Lungs were then lavaged 3× with 0.5 mL of sterile physiological saline, to a total recoverable volume of >1 mL/mouse, placed in clean microcentrifuge tubes. For each mouse 50 μL of BAL fluid was removed and diluted 1:1 with Turk's solution (Merck Chemicals Ltd, UK) in a clean microcentrifuge tube, and retained for undifferentiated leukocyte counts using a Neubauer chamber. Data from each treatment group were used to calculate mean ± standard deviation for each treatment group, respectively. An aliquot of 100 μL undiluted BAL fluid was used for cytospin and differential cell staining (Reastain Quick-Diff Kit, Reagena Ltd, Finland). Differential cell counts were performed using oil emersion under 100× magnification light microscopy. Counts for MNCs and polymorphonuclear cells (PMNs) were performed on 100 and 200 cells per slide, respectively. No other leukocyte types were observed. Data from each treatment group were used to calculate mean ± SD.

Interleukin-6 (IL-6) and tumor necrosis factor alpha (TNF-α) were quantified in the standard BAL supernatant using a colorimetric enzyme-linked immunosorbent assay specific to each cytokine (Mouse TNF-α and IL-6 ELISA Ready-Set-Go! 96-Well plate assay; eBioscience, Cambridge, UK). As a measure of tissue integrity, total protein levels in BAL were quantified using a Quick Start Bradford Protein Assay (Bio-Rad, Hemel Hempstead, UK) according to the manufacturer's instructions. Data were expressed as mean ± SD.

5.5.2 | Lung Edema

The isolated lungs were dissected free of the trachea and connective tissues, then weighed and dried (96 h at 40°C). Dried lungs were reweighed, and both dry lung weight and wet/dry ratio were recorded for standard gravimetric analysis of edema. Data were expressed as mean ± SD.

5.5.3 | Lung Histology

Following formalin fixation, transvers samples of 3 mm thickness were taken from the upper, middle, and lower regions of the left lung. This was followed by dehydration through graded ethanol, then paraffin wax embedding. Serial sections of 4 μm thickness were taken from each region and stained with hematoxylin and eosin (H&E) for cellularity and general morphology, or with picrosirius red stain to detect collagen deposition [23, 43]. For H&E, samples were qualitatively assessed at 40× magnification light microscopy for evidence of macrophage accumulation and vacuolation, PMN infiltration, tissue damage, or remodeling (n = 3–4 animals per group). A semi-quantitative image analysis was performed with picrosirius red stained samples (20× magnification). Total collagen deposition was expressed as the picrosirius factor (PF%), while nonspecific changes, for example, cell infiltration and tissue remodeling, were referred to as the tissue factor (TF%). The PF% was derived by capturing a total of 39 nonoverlapping images (0.6 mm^2 each) across the upper, middle, and lower lung slices for each animal to give a total area per animal of 34 mm^2. The extent of collagen staining (i.e., red

signal) in each 0.6 mm^2 region was quantified using the ImageJ threshold tool (ImageJ software for Microsoft Windows). From the 39 regions imaged, the region with the lowest intensity value, typically associated with non-collagenous tissue, was designated as a background intensity value and subtracted from all other areas to normalize the background signal. Normalized intensities for all 39 sections were then added together, divided by 34 $mm^{2,}$ and multiplied by 100 to yield a PF% value for each animal. Values were reported as the mean ± SD, $n = 3–4$ animals per group.

5.6 | Computed Tomography (CT) Image Acquisition

Mice were anesthetized using isoflurane (2% in O_2). Respiratory rate and temperature were recorded throughout image acquisition, and temperature was maintained by heated air (34°C) in the scanner bed. A Mediso NanoCT scanner was used to obtain transverse helical scans of the thorax at maximum zoom, 360°, pitch 1.0, coincidence 1:4, using a tube voltage of 45 kVp with an exposure time of 1600 ms. Lung density measurements were recorded in Hounsfield units (HU) and the total image acquisition time per mouse was 40 min. All mice underwent CT analysis prior to treatment as a measure of baseline lung health. Following single administration (nanoparticles and vehicles) or the final administration (bleomycin), measurements were taken again at 1, 7, and 28 days post-dosing. The baseline value for each mouse (measurement prior to treatment) was subsequently subtracted from the posttreatment measurements for each time point.

Image analysis was performed using VivoQuantTM software (inviCRO, LLC). For model development and validation, the average density (HU/voxel) from the whole lung of naïve animals was first assessed in comparison to the average density calculated from six evenly spaced transverse lung slices (6 voxel thickness), whereby measurements were restricted to a range of −1000 to −50 HU, which is reflective of the parenchyma [34]. Next, the parenchymal tissue density (HU/voxel) measured between −1000 and −50 HU was compared with the high-density tissue signal (HU/voxel) measured between −300 and +300 HU (associated with the normal vasculature and architecture of the lungs) in the naïve group to ascertain whether high density structures such as airways can be identified with certainty. Individual values were grouped and recorded as mean ± SD ($n = 4$) for either parenchymal or high-density signal analyses. In the analysis of treated versus nontreated animals, the total volume (mm^3) of high-density signals (−300 to +300 HU) from six evenly spaced transverse lung slices was quantified for each mouse at day 0 (prior to treatment) and days 1, 7, and 28 following treatment. Data was also collected from time-matched naïve controls. Baseline values were subtracted from each data set and total high-density signal volumes at each time point plotted as the mean ± SD ($n = 4$).

5.7 | Statistical Analyses

Raw data from analytic comparisons of solid polymers and nanoparticle suspensions were analyzed using an unpaired, two-tailed *t*-test, and results were considered significant at $p < 0.05$ (GraphPad Prism 10 software). Raw data from conventional in vivo treatment protocols were analyzed using two-way ANOVA with (mixed model analysis) with Bonferroni post-test (GraphPad Prism 10 software), and results were considered significant at $p < 0.05$. CT data were analyzed with repeated measures using a Dunnett's test.

Acknowledgments

This work was supported by funding from the C. W. Maplethorpe Trust and the Wellcome Trust. L.A. Dailey would like to thank the European Union Horizon 2020 project IMPTOX (#965173) for support during manuscript preparation. Min-U-Sil 5 quartz dust was a gift from the US Silica company (Houston, TX, USA). The authors wish to thank Dr. Hanpeng Chen for assistance with NMR experiments and Mr. Stephen Clark for assistance in pre-clinical imaging.

Ethics Statement

All research presented conforms to institutional codes of research ethics. Animal studies were performed in accordance with the UK Animals (Scientific Procedures) Act 1986 (Project License Number 70/8279).

Conflicts of Interest

The authors declare no conflicts of interest.

Data Availability Statement

Upon acceptance, data will be made available on Zenodo.

References

1. T. Eberhard, G. Casillas, G. M. Zarus, and D. B. Barr, "Systematic Review of Microplastics and Nanoplastics in Indoor and Outdoor Air: Identifying a Framework and Data Needs for Quantifying Human Inhalation Exposures," *Journal of Exposure Science & Environmental Epidemiology* 34 (2024): 185–196.

2. *Dietary and Inhalation Exposure to Nano- and Microplastic Particles and Potential Implications for human Health* (Geneva: World Health Organization, 2022). Licence: CC BY-NC-SA 3.0 IGO, https://www.who.int/publications/i/item/9789240054608. Accessed on 28.08.2024.

3. N. Ali, J. Katsoulia, E. L. Marczylo, T. W. Gant, S. Wright, and J. B. de la Serna, "The Potential Impacts of Micro-and-Nano Plastics on Various Organ Systems in Humans," *Ebiomedicine* 99 (2024): 104901.

4. S. Yang, T. Zhang, Y. Ge, L. Yin, Y. Pu, and G. Liang, "Inhalation Exposure to Polystyrene Nanoplastics Induces Chronic Obstructive Pulmonary Disease-Like Lung Injury in Mice Through Multi-Dimensional Assessment," *Environmental Pollution* 347 (2024): 123633.

5. J. H. Woo, H. J. Seo, J. Y. Lee, et al., "Polypropylene Nanoplastic Exposure Leads to Lung Inflammation Through p38-Mediated NF-κB Pathway Due to Mitochondrial Damage," *Particle and Fibre Toxicology* 20 (2023): 2.

6. Y. Ji, L. Chen, Y. Wang, et al., "Realistic Nanoplastics Induced Pulmonary Damage via the Crosstalk of Ferritinophagy and Mitochondrial Dysfunction," *ACS Nano* 18, no. 26 (2024): 16790–16807.

7. M. C. Jones, S. A. Jones, Y. Riffo-Vasquez, et al., "Quantitative Assessment of Nanoparticle Surface Hydrophobicity and Its Influence on Pulmonary Biocompatibility," *Journal of Controlled Release* 183, no. 1 (2014): 94–104.

8. L. A. Dailey, R. Hernández-Prieto, A. M. Casas-Ferreira, et al., "Adenosine Monophosphate Is Elevated in the Bronchoalveolar Lavage Fluid of Mice With Acute Respiratory Toxicity Induced by Nanoparticles With High Surface Hydrophobicity," *Nanotoxicology* 9, no. 1 (2015): 106–115.

9. S. Y. Seong and P. Matzinger, "Hydrophobicity: An Ancient Damage-Associated Molecular Pattern That Initiates Innate Immune Responses," *Nature Reviews Immunology* 4, no. 6 (2004): 469–478.

10. D. F. Moyano, M. Goldsmith, D. J. Solfiell, et al., "Nanoparticle Hydrophobicity Dictates Immune Response," *Journal of the American Chemical Society* 134, no. 9 (2012): 3965–3967.

11. A. Woods, A. Patel, D. Spina, et al., "In Vivo Biocompatibility, Clearance, and Biodistribution of Albumin Vehicles for Pulmonary Drug Delivery," *Journal of Controlled Release* 210 (2015): 1–9.

12. A. Patel, A. Woods, Y. Riffo-Vasquez, et al., "Lung Inflammation Does Not Affect the Clearance Kinetics of Lipid Nanocapsules Following Pulmonary Administration," *Journal of Controlled Release* 235 (2016): 24–33.

13. J. A. Brydson, *Poly(vinyl acetate) and Its Derivatives in Plastics Materials*, 7th ed. (London: Butterworth-Heinemann, 1999), 386–397.

14. B. Graca, K. Szewc, D. Zakrzewska, A. Dołęga, and M. Szczerbowska-Boruchowska, "Sources and Fate of Microplastics in Marine and Beach Sediments of the Southern Baltic Sea—A Preliminary Study," *Environmental Science and Pollution Research* 24 (2017): 7650–7661.

15. F. Liu, K. B. Olesen, A. R. Borregaard, and J. Vollertsen, "Microplastics in Urban and Highway Stormwater Retention Ponds," *Science of the Total Environment* 671 (2019): 992–1000.

16. M. O. Gul, S. A. Jones, L. A. Dailey, et al., "A Poly(vinyl alcohol) Nanoparticle Platform for Kinetic Studies of Inhaled Particles," *Inhalation Toxicology* 21, no. 7 (2009): 631–640.

17. J. Chana, B. Forbes, and S. A. Jones, "The Synthesis of High Molecular Weight Partially Hydrolysed Poly(vinyl alcohol) Grades Suitable for Nanoparticle Fabrication," *Journal of Nanoscience and Nanotechnology* 8, no. 11 (2008): 5739–5747.

18. S. A. Jones, S. Mesgarpour, J. Chana, and B. Forbes, "Preparation and Characterisation of Polymeric Nanoparticles Using Low Molecular Weight Poly(vinyl alcohol)," *Journal of Biomedical Nanotechnology* 4, no. 3 (2008): 319–325.

19. E. Hoffman, A. Kumar, V. Kanabar, et al., "In Vitro Multiparameter Assay Development Strategy Toward Differentiating Macrophage Responses to Inhaled Medicines," *Molecular Pharmaceutics* 12, no. 8 (2015): 2675–2687.

20. A. Kumar, E. M. Bicer, A. Babin Morgan, et al., "Enrichment of Immunoregulatory Proteins in the Biomolecular Corona of Nanoparticles Within Human Respiratory Tract Lining Fluid," *Nanomedicine Nanotechnology Biology and Medicine* 12 (2016): 1033–1043.

21. M. Roursgaard, S. S. Poulsen, L. K. Poulsen, et al., "Time-Response Relationship of Nano and Micro Particle Induced Lung Inflammation. Quartz as Reference Compound," *Human & Experimental Toxicology* 29, no. 11 (2010): 915–933.

22. A. L. Babin, C. Cannet, C. Gérard, D. Wyss, C. P. Page, and N. Beckmann, "Noninvasive Assessment of Bleomycin-Induced Lung Injury and the Effects of Short-Term Glucocorticosteroid Treatment in Rats Using MRI," *Journal of Magnetic Resonance Imaging* 33, no. 3 (2011): 603–614.

23. A. L. Babin, C. Cannet, C. Gérard, et al., "Bleomycin-Induced Lung Injury in Mice Investigated by MRI: Model Assessment for Target Analysis," *Magnetic Resonance in Medicine* 67, no. 2 (2012): 499–509.

24. N. Beckmann, B. Tigani, L. Mazzoni, and J. R. Fozard, "Techniques: Magnetic Resonance Imaging of the Lung Provides Potential for Non-Invasive Preclinical Evaluation of Drugs," *Trends in Pharmacological Sciences* 24, no. 10 (2003): 550–554.

25. N. Beckmann, C. Cannet, H. Karmouty-Quintana, et al., "Lung MRI for Experimental Drug Research," *European Journal of Radiology* 64, no. 3 (2007): 381–396.

26. N. L. Ford, H. N. Nikolov, C. J. D. Norley, et al., "Prospective Respiratory-Gated Micro-CT of Free Breathing Rodents," *Medical Physics* 32, no. 9 (2005): 2888.

27. N. L. Ford, E. L. Martin, J. F. Lewis, R. A. W. Veldhuizen, M. Drangova, and D. W. Holdsworth, "In Vivo Characterization of Lung Morphology and Function in Anesthetized Free-Breathing Mice Using Micro-Computed Tomography," *Journal of Applied Physiology* 102, no. 5 (2007): 2046–2055.

28. B. A. Simon, G. E. Christensen, D. A. Low, and J. M. Reinhardt, "Computed Tomography Studies of Lung Mechanics," *Proceedings of the American Thoracic Society* 2, no. 6 (2005): 517–521.

29. D. M. Brown, M. R. Wilson, W. MacNee, V. Stone, and K. Donaldson, "Size-Dependent Proinflammatory Effects of Ultrafine Polystyrene Particles: A Role for Surface Area and Oxidative Stress in the Enhanced Activity of Ultrafines," *Toxicology and Applied Pharmacology* 175, no. 3 (2001): 191–199.

30. R. Duffin, L. Tran, D. Brown, V. Stone, and K. Donaldson, "Proinflammogenic Effects of Low-Toxicity and Metal Nanoparticles In Vivo and In Vitro: Highlighting the Role of Particle Surface Area and Surface Reactivity," *Inhalation Toxicology* 19 (2007): 849–856.

31. X. Zhou, W. Jin, and J. Ma, "Lung Inflammation Perturbation by Engineered Nanoparticles," *Frontiers in Bioengineering and Biotechnology* 11 (2023): 1199230.

32. J. Casey, J. Kaplan, E. N. Atochina-Vasserman, et al., "Alveolar Surfactant Protein D Content Modulates Bleomycin-Induced Lung Injury," *American Journal of Respiratory and Critical Care Medicine* 172, no. 7 (2005): 869–877.

33. S. Murakami, N. Nagaya, T. Itoh, et al., "Prostacyclin Agonist With Thromboxane Synthase Inhibitory Activity (ONO-1301) Attenuates Bleomycin-Induced Pulmonary Fibrosis in Mice," *American Journal of Physiology. Lung Cellular and Molecular Physiology* 290, no. 1 (2006): L59–L65.

34. Z. Zhou, J. Kozlowski, and D. P. Schuster, "Physiologic, Biochemical, and Imaging Characterization of Acute Lung Injury in Mice," *American Journal of Respiratory and Critical Care Medicine* 172, no. 3 (2005): 344–351.

35. D. Richards and A. Ivanisevic, "Inorganic Material Coatings and Their Effect on Cytotoxicity," *Chemical Society Reviews* 41, no. 6 (2012): 2052.

36. W. Wohlleben, M. D. Driessen, S. Raesch, et al., "Influence of Agglomeration and Specific Lung Lining Lipid/Protein Interaction on Short-Term Inhalation Toxicity," *Nanotoxicology* 10, no. 7 (2016): 970–980.

37. A. Valsesia, C. Desmet, I. Ojea-Jiménez, et al., "Direct Quantification of Nanoparticle Surface Hydrophobicity," *Communications Chemistry* 1 (2018): 53.

38. N. Anderson and J. Borlak, "Drug-Induced Phospholipidosis," *FEBS Letters* 580, no. 23 (2006): 5533–5540.

39. S. Martinez Legaspi and L. Segatori, "Aggregation Behavior of Nanoparticle-Peptide Systems Affects Autophagy," *Bioconjugate Chemistry* 30, no. 7 (2019): 1986–1997.

40. Y. Li and D. Ju, "The Role of Autophagy in Nanoparticles-Induced Toxicity and Its Related Cellular and Molecular Mechanisms," *Advances in Experimental Medicine and Biology* 1048 (2018): 1–84.

41. S. T. Stern, P. P. Adiseshaiah, and R. M. Crist, "Autophagy and Lysosomal Dysfunction as Emerging Mechanisms of Nanomaterial Toxicity," *Particle and Fibre Toxicology* 9, no. 1 (2012): 20.

42. W. Y. Zhong, M. Lü, L. Y. Liu, et al., "Autophagy as New Emerging Cellular Effect of Nanomaterials," *Chinese Science Bulletin* 58, no. 33 (2013): 4031–4038.

43. C. Egger, C. Cannet, C. Gérard, et al., "Administration of Bleomycin via the Oropharyngeal Aspiration Route Leads to Sustained Lung Fibrosis in Mice and Rats as Quantified by UTE-MRI and Histology," *PLOS ONE* 8, no. 5 (2013): e63432.

44. S. Chicklore, V. Goh, M. Siddique, A. Roy, P. K. Marsden, and G. J. R. Cook, "Quantifying Tumour Heterogeneity in 18F-FDG PET/CT Imaging by Texture Analysis," *European Journal of Nuclear Medicine and Molecular Imaging* 40, no. 1 (2013): 133–140.

45. C. Kavitha, B. P. Rao, and A. Govardhan, "Image Retrieval Based on Color and Texture Features of the Image Sub-Blocks," *International Journal of Computer Applications* 15, no. 7 (2011): 33–37.

46. M. G. Lubner, A. D. Smith, K. Sandrasegaran, D. V. Sahani, and P. J. Pickhardt, "CT Texture Analysis: Definitions, Applications, Biologic Correlates, and Challenges," *Radiographics* 37, no. 5 (2017): 1483–1503.

47. Y. Ohno, K. Aoyagi, D. Takenaka, et al., "Machine Learning for Lung Texture Analysis on Thin-Section CT: Capability for Assessments of Disease Severity and Therapeutic Effect for Connective Tissue Disease Patients in Comparison With Expert Panel Evaluations," *Acta Radiologica* 63, no. 10 (2022): 1363–1373.

48. E. F. Redente, K. W. Kopf, A. N. Bahadur, A. Robichaud, L. K. Lundblad, and L. T. McDonald, "Application-Specific Approaches to MicroCT for Evaluation of Mouse Models of Pulmonary Disease," *PLOS ONE* 18, no. 2 (2023): e0281452.

49. K. J. Field and C. M. Lang, "Hazards of Urethane (ethyl carbamate): A Review of the Literature," *Laboratory Animals* 22, no. 3 (1988): 255–262.

50. IARC Working Group, *Re-Evaluation of Some Organic Chemicals, Hydrazine and Hydrogen Peroxide (Part 1, Part 2, Part 3)*, vol. 71 (Lyon, France: IARC Press, 1999).

Supporting Information

Additional supporting information can be found online in the Supporting Information section.